Bioactive Constituents, Metabolites, and Functions

Cuprizone-induced demyelination in mouse hippocampus is alleviated by ketogenic diet

Chunhong Liu, Ning Zhang, Ruiyan Zhang, Li Jin, Athanasios K. Petridis, Gabriele Loers, Xuexing Zheng, Zhengping Wang, and Hans-Christian Siebert

J. Agric. Food Chem., **Just Accepted Manuscript** • DOI: 10.1021/acs.jafc.0c04604 • Publication Date (Web): 12 Sep 2020

Cuprizone-induced demyelination in mouse hippocampus is alleviated by ketogenic diet

Chunhong Liu[&], Ning Zhang[&*], Ruiyan Zhang[&*], Li Jin[&], Athanasios K. Petridis[$], Gabriele Loers[‡*], Xuexing Zheng[§], Zhengping Wang[&], Hans-Christian Siebert[†]

[&] Institute of Biopharmaceutical Research, Liaocheng University, Liaocheng, Shandong 252000, China.

[$] Heinrich Heine University, Neurosurgical Department, University of Düsseldorf, Moorenstraße 5, 40255 Düsseldorf, Germany.

[‡] Center for Molecular Neurobiology Hamburg, University Medical Center Hamburg-Eppendorf, University of Hamburg, Falkenried 94, 20251 Hamburg, Germany.

[§] Department of Virology, School of Public Health, Shandong University, Jinan 250012, China

[†] RI-B-NT - Research Institute of Bioinformatics and Nanotechnology, Schauenburgerstr. 116, 24118 Kiel, Germany.

Corresponding author:

1. N. Zhang: zhangning1111@126.com

2. R. Zhang: zry147896@163.com

3. G. Loers: gabriele.loers@zmnh.uni-hamburg.de

Abstract

Multiple sclerosis (MS) is a chronic inflammatory demyelinating disease of the central nervous system (CNS). Recently, ketogenic diet (KD) supplementation has attracted great interests. Therefore, we established the cuprizone (CPZ)-induced demyelination mouse model, to investigate the possible neuroprotective effect of KD on the hippocampus of mice. We found that KD significantly elevated the level of serum β-hydroxybutyric acid and improved behavioral, motor abnormalities, impaired spatial learning and memory of CPZ-induced demyelination mice. Meanwhile, KD lessened the hippocampal demyelination by enhancing the expression of mature oligodendrocytes (OLs), which was revealed by the elevated expression of MBP and CNPase, as well as the luxol fast blue-staining intensity. Furthermore, KD inhibits the activation of microglia (especially M1-liked microglia) and reactive astrocytes. Interestingly, KD attenuated the CPZ-induced oxidative stress by decreasing the malondialdehyde (MDA) content and restoring the glutathione (GSH) levels. In addition, the double immunofluorescence staining revealed that KD enhanced the expression of SIRT1 in astrocytes, microglia and mature oligodendrocytes. Concomitantly, western blot demonstrated that KD increased the expression of SIRT1, phosphorylated-AKT, mTOR and PPAR-γ. In conclusion, KD exerted a neuroprotective effect on CPZ-induced demyelination mice and this activity was associated with the modulation of the SIRT1/PPAR-γ and SIRT1/P-Akt/mTOR pathways.

Keywords: multiple sclerosis, ketogenic diet, demyelination, hippocampus, SIRT1

Introduction

Multiple sclerosis (MS) is a chronic inflammatory disorder of the central nervous system (CNS) and is a debilitating and demyelinating disease.[1] Up to present time, the treatments for MS include immunomodulatory, immunosuppressive and antibody mediated approaches, while these are only partially effective, or have side effects.[2,3] Therefore, new strategies are being developed to slow down MS progression. Among these complementary approaches, ketogenic diet (KD) has gained increasing attention for the treatment of MS.[4,5] KD is a high fat, low carbohydrate and adequate protein diet, which leads to the production of ketone bodies within the liver for producing adenosine triphosphate (ATP).[6] Recently, clinical trials in patients with MS have revealed that medium chain triglycerides (MCT)-KD can improve learning and memory of these individuals.[7] Although KD supplements were taken by MS patients,[8] available data at present are insufficient to clearly explain the mechanism. Thus, more research is still required in this field.

During myelin regeneration, OPCs need to be recruited into the lesioned area, and differentiated into myelin-associated oligodendrocytes (OLs). Previous studies have reported that the poor remyelination in MS may be partly due to the neuroinflammation, which results in myelin dysfunction and poor regeneration of the glial scar.[9] Excessive activation of microglia is associated with secretion of a large amounts of pro-inflammatory cytokines, as well as the release of neurotoxic substances, and nitric oxide, thereby aggravating the damage of neurons and myelin loss.[10] In addition, reactive astrocytes inhibit the migration of OPCs to the lesion site by secreting chemokine such as MIP-3α (CCL-20), and thereby promote demyelination.[11] Futhermore, myelination failure is associated with axon damage, which leads to deficits in cognition (e.g. memory and attention). Cuprizone (CPZ) is a compound that can mimic toxic demyelination of

MS.[12,13] The CPZ-induced demyelination model exhibited white matter deficits, astrocyte and microglia activation, as well as cognitive impairments and few motor function deficits. Therefore, this is a suitable animal model for the present study, to explore the effects of KD on behavioral abnormalities, myelination and neuroinflammation.[14,15]

Accumulating data has revealed that oxidative stress serves an important role in MS pathogenesis. Several antioxidant enzymes such as superoxide dismutase (SOD), glutathione peroxidase (GPX) and catalase responsible for scavenging cellular ROS. Recent studies have reported that mice exposed to CPZ exhibit enhanced oxidative stress, which is characterized by the decreased activity of GSH-Px, and the increased concentration of MDA.[16] Interestingly, KD treatment ameliorated the experimental autoimmune encephalomyelitis (EAE, a murine model for MS)-induced cognitive deficits in mice by attenuating the robust immune response and oxidative stress.[17] However, it remains poorly understood whether KD can improve the clinical symptoms and cognitive impairment in CPZ-induced demyelination partly by suppressing oxidative stress.

Silent mating type information regulation 2 homologue 1 (SIRT1), which is a member of the sirtuin family, has been shown to have neuroprotective effects in neurodegenerative diseases. Several studies have indicated that SIRT1 plays an indispensable role in modulating neuronal plasticity and cognitive function.[18,19] Importantly, the SIRT1-dependent deacetylation of the pH domain of Akt is necessary for the activation of the protein.[20]. SIRT1 can promote the phosphorylation and activation of Akt.[21] Several lines of evidence have demonstrated that SIRT1 plays a neuroprotective role by inhibiting the oxidative stress pathway.[22] Recent findings have revealed that the remyelination of EAE model mice is increased by activating the phosphatidylinositol 3-kinase (PI3K)/Akt/mTOR signaling pathway, which is necessary for

oligodendrocyte survival and axon myelination.[23] In addition, mTOR activation can promote the differentiation of OPCs into mature OLs and enhance the myelination in the brain.[24] Remarkably, some studies have confirmed that peroxisome proliferator-activated receptor (PPAR-γ) can promote the recovery from demyelination through its direct effect on OLs.[25]

In the brain, the hippocampus play a crucial role in learning and memory. Dysfunction of the hippocampus may cause cognitive defects. MS-associated cognitive dysfunction appears early during the course of the disease. Demyelination is one of the hallmarks in MS. However, so far, the complex pathological mechanism of hippocampal damage caused by demyelination has not been well revealed. Therefore, we analyze in detail the neuroprotective effect of KD on CPZ-induced demyelination in the hippocampus, and to identify the potential underlying mechanisms.

Materials and methods

Animals

Male C57BL/6 mice (7 weeks old) were obtained from the Jinan Pengyue Experimental Animal Company (Jinan, China). The mice were housed under normal environmental conditions (22 ± 2°C) with 12 hours/12 hours light/dark cycles and fed ad libitum. Animals procedures were performed in accordance with the Guidelines for Care and Use of Laboratory Animals of Shandong University and the animal studies in this research waere approved by the Animal Ethics Committee of Shandong University (permit number 20191018).

Experimental design

In order to induce demyelination, mice were given 0.2% (w/w) CPZ (Sigma-Aldrich Inc., St. Louis, MO, USA) mixed into a regular diet of ground standard rodent chow for 5 weeks. The

animal subjects were randomly assigned into three groups (A) ND group, mice were fed with normal diet; (B) CPZ+ND group, mice were fed with normal diet with 0.2 % CPZ; (C) CPZ+KD group, mice in the KD (Table 1)-administered groups were fed with CPZ, n=8 animals per group.

All mice received a nutritionally balanced diet provided by the animal feed manufacturer Beijing HFK Bioscience CO., LTD (Beijing, China). KD was performed as previously described by Hao et al., the ratio of 3:1 for fat:nonfat (protein and carbohydrates).[26] In brief, the aim of KD was to induce ketosis. Micronutrient composition of the KD used in the current experiment is listed in Table 1.

Body weight

During the entire test period, body weights was measured at 8:00-9:00 in the morning every two days.

Behavioral and cognitive tests

Open field test (OF)

The OF was performed as previously described by Zhang et al.[27] The arena was lit by lightemitting diode lightings placed above the arena. The mouse was placed in the center of the open field box (45 cm long × 45 cm wide × 30 cm high), with a short, one minute explore the maze and then mice were monitored for fives minutes in the square open field with a video tracking software. After testing each mouse, wipe the field and spray with alcohol to avoid disturbing the results. The analysis of OF was carried out by SMART 3.0 (Panlab Harvard Apparatus, Spain).

Rotarod test (RT)

Motor coordination and balance were evaluated using a rotarod apparatus (Panlab, Barcelona, Spain). The RT was performed as previously described by Janssen et al.[28] The length of time that the animals were able to stay on the device was recorded as latency to fall (seconds). The mice were subjected to three trials at accelerating speeds from 4 rpm to 40 rpm. In each experiment, latency to fall was measured. Animals rested for 30 minutes between trials to avoid fatigue. The average latency time of three trials was calculated for the analysis.

Morris water maze (MWM)

MWM is a test which forces experimental animals to swim and learn to find a hidden platform in the water. It is most commonly used to test the spatial memory. The MWM for both practice and testing purposes was designed using SMART 3.0 (Panlab Harvard Apparatus, Spain). The MWM consisted of a circular pool (diameter of 120 cm, depth of 36 cm) and was filled with water to a depth of 30 cm and maintained at 22 ± 1°C. The water maze area was divided into four equal quadrants (N, S, E and W) with equal size and release points were designed at each quadrant. The escape platform was submerged 2 cm below the water surface and located in the center of the northeast quadrant. MWM was done according to a previously published protocol,[29] the hidden platform task was given four times a day for five consecutive days. Mice remained on the platform for 15 seconds and then removed from the tank. If a mouse failed to find the platform within 60 seconds, it was gently guided to it. The animals were allowed to stay on the platform for 15 seconds until the next experiment began. On day six, the platform was removed and each mouse was allowed to swam freely for 60 seconds. Distance to target, the number of platform crossings and the time spent in the target quadrant were calculated by computer software.

Tissue preparation

Upon euthanasia, the mice were treated with ketamine and xylazine by intravenous injection, each mouse was perfused with PBS and the brain was extracted at the study end point on day 35. Brains were washed with ice-cold phosphate buffered saline (PBS) as previously described.[30] Then, some mouse brains were dissected and immersed in 4 % paraformaldehyde (PFA) for 24 hours, 5 μm thick sections from brain samples were prepared from paraffin-embedded blocks. Some mouse brains were used for isolation of the hippocampus. The isolated hippocampi were used immediately or preserved at -80℃.

Biochemical parameters

Measurement of blood ketone body and determination of β-hydroxybutyric acid levels in hippocampus

Every 7 days from the start of the experiment, tail-vein blood ketone body was measured under the fed state, using a handheld ketone meter (Blood ketone body tester, T-1, Beijing Yicheng bioelectronics Co., Ltd Beijing, China).[31] All the samples were taken at the same time. At day 35, mouse brains were removed and the hippocampus was separated. Hippocampal homogenate was then prepared. The supernatant was collected at 1,000 × g for 20 minutes. The concentration of β-hydroxybutyric acid in the hippocampus was detected by mouse β-hydroxybutyric acid ELISA kit (Shanghai Jianglai Industrial Limited By Share Ltd, China), according to manufacturer's protocol.

Serum aspartate aminotransferase (AST), alanine aminotransferase (ALT), nitrogen creatinine (Cr) and blood urea nitrogen (BUN) detection

AST, ALT, Cr and BUN ELISA kits were purchased from Nanjing Jiancheng Bioengineering Institute (Nanjing, China). The blood was collected into microvette tubes (EDTA free) and

centrifuged at 1,300 × g for 10 minutes. The isolated serum samples were transferred to Eppendorf tubes. The transaminase activity, serum creatinine and urea nitrogen concentration in serum were measured according to the manufacturers instructions. Light absorbance was measured with an ultraviolet light-visible spectrophotometer (U-3900H, Hitachi Corporation, Japan) at the corresponding wavelengths.[32]

Measurement the GSH-Px, GSH, and MDA levels in hippocampus

Hippocampi were homogenized with cold Tris-HCl buffer (pH 7.4) to obtain 10% homogenate (w/v). The activity of GSH-Px, and content of GSH and MDA were determined following the manufacturer's recommendations. GSH-Px assay kit, GSH assay kit and MDA assay kit were obtained from Nanjing Jiancheng Bioengineering Institute (Nanjing, China).

Histopathological examination

Hematoxylin and eosin (H&E) staining

The brain sections were deparaffinized in xylene and rehydrated in a graded ethanol series (100%, 90%, 75%). The brain sections washed in PBS three times, each time for 5 minutes. Then the sections were stained with H&E for histopathology.[33]

Nissl staining

The brain sections were first hydrated in Milli-Q water for 20 minutes and then placed under agitation in cresyl violet staining solution for 10 minutes before being rinsed in Milli-Q water. Brain slices were rehydrated in a descending ethanol series (75%, 90%, 100%). Slices were cleared in xylene for 5 minutes before being covered with neutral balsam and coverslip.[34]

Immunohistochemistry and immunofluorescence double-labeling

Immunohistochemistry

Paraffin embedded sections were de-waxed and rehydrated, and microwaved for 20 minutes in 10 mM citrate buffer (pH 6.0) for antigen retrieval. Endogenous peroxidase activity was quenched by 3% hydrogen peroxide, and slides were washed with PBS and then blocked with 20 % normal goat serum for 20 miuntes. Then the sections were incubated overnight at 4°C with specific primary antibodies.[35] The primary antibodies used are described in Table 2. Secondary biotinylated goat anti-rabbit IgG (H+L) were applied at a 1:500 dilution (Proteintech, USA) for 2 hours at room temperature, and an avidin-biotin-peroxidase complex kit (ABC Kit, Vector Laboratories, Burlingame, UK) was used for immunostaining. Cell counting in the hippocampus was performed using Image J (NIH) and calculated by the average value. The microphotographs were taken on a Leica DMLB microscope at 40 × magnification.[36]

Immunofluorescence double-labeling

Immunofluorescence double-labeling was used to identify cells that express SIRT1.[37] Briefly, dewaxed paraffin sections were subjected to heat-mediated antigen retrieval (citrate buffer, pH 6.0). Brain sections were co-incubated with mouse anti-SIRT1 (Abcam, 1:200), rabbit anti-NG2 (Merck; 1:400), rabbit anti-CNPase (Merck; 1:200), rabbit anti-Iba-1 (Abcam;1:50), rabbit anti-GFAP (Millipore, 1:500), overnight at 4°C. The following day, the sections were washed 3 times with fresh PBS for 3 minutes each, and incubated with FITC 488-conjugated secondary antibody (goat anti-mouse, 1:100)/Cy3-conjugated secondary antibody (goat anti-rabbit, 1:100) in the dark for 1 hour at room temperature. Nuclei were counterstained with 4′,6′-diamidino-2-phenylindole (DAPI, 0.5 μg/ml) at room temperature. After washing 3 times with fresh PBS for 3 minutes each, the sections were mounted in Dako Fluorescence Mounting

Medium (S3023, Dako Cytomation GmbH, Hamburg, Germany) and sealed with cover slips. All images were taken using a Nikon Eclipse Ti-E epifluorescence inverted microscope.

Western blot

The hippocampus was lysed for total protein extraction by Minute™ Total Protein Extraction Kit (Invent Biotechnologies). The concentration of protein was measured by BCA Protein Assay Kit (Sheng gong® Sangon Biotech). Sodium dodecyl sulfate-polyacrylamide gel electrophoresis (SDS-PAGE) was uesed to separate the proteins (25 μg) from each sample and then electrophoretically transferred to polyvinyl difluoride membranes by electrophoresis (Millipore, Billerica, MA, USA). The membrane was blocked in 5% skim milk in Tris-buffered saline solution pH 7.4 for 2 hours at room temperature and incubated with the primary antibody at 4°C overnight. The following antibodies were used: rabbit anti-CNPase (Proteintech, 1:10,000), mouse anti-SIRT1 (Millipore Corporate, 1:2,000), rabbit anti-*p*-Akt (Ser473) (Abcam, 1:125), rabbit anti-mTOR (Abcam, 1:2,000), rabbit anti-PPAR-γ (Abcam, 1:800), β-actin (Proteintech, 1:10,000), GAPDH (Ambion, 1:20,000). The following day, the membranes were washed with TBST for 5 minutes × 3 times, and incubated with secondary antibody (goat anti-rabbit/goat anti-mouse IgG) conjugated with horseradish peroxidase at a dilution of 10,000 (MultiSciences) for 1 hour (room temperature) and washed three times with TBST. The proteins were determined using an ECL western blot detection kit (Amersham Biosciences, NJ, USA). Band density traces and quantification were determined and the expression levels of these proteins were quantified by comparison with the levels of ND.

Statistical analysis

All statistical analyses were carried out in SPSS 25.0 software. Data were reported as mean ± error of the mean (SEM). One-way analysis of variance (ANOVA) with Tukey post hoctest (for multiple comparisons) was used for the comparison among groups. P value less than 0.05 was considered statistically significant. As compared with the ND groups: *P<0.05, **P<0.01, ***P<0.001; as compared with the CPZ+ND groups: $^{\#}$P<0.05, $^{\#\#}$P<0.01, $^{\#\#\#}$P<0.001.

Results

Effect of KD on CPZ-induced alterations in body weight

A significant reduction in body weight was found in the KD group in comparison with ND group (Figure 1). The present study demonstrated that CPZ intoxication caused a significant decrease in the body weight of mice. Interestingly, compared to mice in the CPZ+ND group, the body weight of mice in the CPZ+KD group significantly increased from day four, up to the end of experiment (Figure 1, P<0.001).

Behavioral tests

OF

The decrease in exploration and increase in anxiety of mice have been reported in the CPZ models.[38,39] The present study showed that mice in the CPZ+ND group traveled shorter distance at the center area and in the overall area of the apparatus, when compared to mice in the ND group (Figures 2A-2C). Futhermore, the time spent in the central area was significantly lower in the CPZ+ND group, when compared to the ND group (Figures 2A and 2D, P<0.001), Interestingly, the central area travel distance, total distance and time spent were all significantly increased in KD-treated mice, when compared to mice in the CPZ+ND group (Figure 2). These data suggests

253 that KD decreases the anxiety-like behavior, thereby increasing the exploratory behavior of mice
254 by promoting remyelination.

255 The RT was designed to assess the motor coordination of mice. The motor coordination and
256 balance were monitored using the accelerated rotarod test after mice were fed with CPZ for five
257 weeks. Consistent with a previous study,[40] we found that mice in the CPZ+ND group had a
258 significantly reduced mean latency to fall on the rotarod apparatus, when compared to the ND
259 group (Figure 2E, $P<0.001$), suggesting that CPZ-intoxication indeed impairs motor coordination.
260 When compared to the ND group, KD treated mice stayed significantly longer on the rotarod
261 apparatus (Figure 2E, $P<0.001$). However, there was no difference between the ND group and
262 CPZ+KD group. These results indicate that KD treatment prevented the motor deficits induced by
263 CPZ.

264 The learning and memory impairment of mice that received CPZ were assessed using the
265 MWM test. On day six of the MWM test, learning and memory were assessed during the probe
266 trial (Figure 2F). Mice in the ND+CPZ group traveled longer distances to the target, when
267 compared to control mice (Figures 2F and 2G, $P<0.001$). Furthermore, compared to the control
268 group, the platform crossing times and platform quadrant residence duration of mice significantly
269 decreased in the CPZ-treated group (Figures 2F, 2H and 2I; $P<0.001$). In addition, decreased
270 distance to target, and increased platform crossing time and platform quadrant residence time were
271 observed in KD-treated mice, when compared to mice in the CPZ+ND group (Figures 2G-2I,
272 $P<0.01$). These findings suggest that KD can recover the CPZ-induced learning and memory
273 deficits.

274 **Biochemical parameters**

The level of blood ketone body and β-hydroxybutyrate acid in hippocampi of mice significantly increased in the CPZ+KD group, when compared to the CPZ+ND and ND groups (Figures 3A and 3B, $P<0.001$). The levels of AST, ALT, Cr and BUN in mice were determined after five weeks of CPZ induction. No significant differences were observed (Figures 3C-3F). These results suggest that all animals had normal liver and kidney function.

Demyelination quantification

To assess the content of myelin in the hippocampus, the myelination was evaluated by MBP immunohistochemistry. As shown in Figures 4A, 4B and 4C, the CPZ fed in mice caused a marked demyelination in the hippocampus. Compared with the ND group, CA1, CA2 and CA3 region of the hippocampus suffered from severe myelin loss in the CPZ+ND group (Figures 4A-4B3). However, the MBP immunohistochemistry revealed an increased staining of fibers, which typically appeared disc-like, compact, and at times extended radially in the marked areas of the hippocampus, after KD administration (Figures 4A-4C3). Furthermore, the analysis of the hippocampal sections demonstrated the significantly elevated immunodensity of MBP in KD-treated mice when compared with the CPZ+ND group, at day 35 (Figure 4E, $P<0.05$), suggesting that KD plays an important role in protecting the myelin sheet.

NG2 glia residing at or close to demyelination lesions function as oligodendrocyte precursor cells or some extent generate astrocytes after CNS insults. In the present study, CPZ+ND group showed an increased in the number of $NG2^+$ OPCs in comparison to control group ($P<0.001$). While, KD treatment significantly reduced the number of $NG2^+$ OPCs in CPZ mice (Figures 4D and 4F). CNPase is a myelin-associated enzyme expressed exclusively by differentiating OLs. A decreased expression of CNPase in the hippocampus was found in mice that received CPZ, and a

certain extent of protection was observed in KD treated mice at five weeks post-induction (Figures 4G and 4H). The demyelinating areas in the hippocampus were filled with $NG2^+$ OPCs in mice receiving CPZ, indicating that the recruitment of $NG2^+$ OPCs to the lesions was normal, but these OPCs might have difficulties to differentiate into mature OLs. Furthermore, the KD treatment protected myelin sheaths by promoting the differentiation of OPCs into mature OLs.

Morphology of the hippocampus

H&E staining in the hippocampus was performed to detect the neuronal integrity and orderliness. The general morphology of the hippocampus and neurons in the ND group was well-preserved (Figure 5A). The area marked with a black box represents the DG area of the hippocampus. Figure 5B presents the partial enlargement of Figure 5A. As shown in Figure 5B, neuron atrophy was found in the DG of the hippocampus of mice after receiving CPZ. Furthermore, the arrangement of hippocampal neurons in mice in the CPZ+ND group was irregular, while a normal neuronal morphology was observed in the hippocampal DG area of mice after treatment with KD (Figure 5B).

Nissl staining was utilized to evaluate the effects of CPZ-induced typical neuropathological changes in the hippocampus. These present results revealed that the arrangement of granular neurons in the dentate gyrus in the ND group was relatively linear, and the Nissl bodies were abundant. The CPZ+ND group appeared to have neuronal pyknosis and disorganized neuronal layering as compared to the ND group, while KD treatment exhibited a recovering effect on hippocampal neuronal damage.

Effects of KD on microglia in the CPZ-induced demyelination model

318 Microglia activation was visualized using CD68 immunohistochemical staining, and microglia
319 polarization was investigated in the hippocampus by CD16/32 immunohistochemistry staining
320 (representing the M1-liked microglia). It has been reported that microglia are activated in mice
321 after receiving CPZ, especially M1 phenotype microglia.[41,42] M1 microglia can produce
322 proinflammatory cytokines, such as IL-1β, IL-6 and TNF-α, which subsequently enhance myelin
323 loss. Remarkably, in the hippocampus, the number of $CD68^+$ cells (representing activated
324 microglia, Figures 6A and 6C, $P<0.001$) and $CD16/32^+$ cells (Figures 6B and 6D, $P<0.001$) both
325 increased after five weeks of feeding with CPZ, while the number of $CD68^+$ cells and $CD16/32^+$
326 cells decreased after KD administration (Figures 6C and 6D, $P<0.001$). These present findings
327 suggest that KD can inhibit the CPZ-induced activation of microglia, and especially reduce the
328 number of M1-like microglia.

329 **Effects of KD on astrocyte activation in the CPZ-induced demyelination model**

330 Immunohistochemical staining of GFAP was used to evaluate astrogliosis. Gudi et al. reported
331 that astrocytes are activated in mice after receiving CPZ.[43] Consistent with other previously
332 reported studies, the number of $GFAP^+$ cells was significantly higher in the CPZ+ND group than
333 in the ND group. However, after five weeks post-induction, the KD treatment group exhibited
334 fewer $GFAP^+$ cells in the hippocampus, and a significant decrease in the number of $GFAP^+$ cells
335 was observed in the CPZ+KD group (Figure 7C, $P<0.001$). Reactive astrogliosis manifested
336 through the significant increase in GFAP immunoreactivity, which is clearly visible around the
337 lesioned hippocampal area in mice that received CPZ (Figures 7A and 7B). Figure 7B presents the
338 magnification of the black-labeled box in Figure A, which marks the CA3 region of the
339 hippocampus. As shown in Figure 7B, the morphology of reactive astrocytes revealed that there

was less swelling in the hippocampus of KD-treated mice, when compared to CPZ mice. Evidence has revealed that astrocytes play an important role in neuronal resilience and remyelination in the CNS.[44] During the development of the CNS, astrocytes secrete axonal growth factors and release various neurotrophic factors, such as nerve growth factor (NGF) and basic fibroblast growth factor (bFGF), to maintain the survival of neurons and to promote the growth of neuronal processes.[45,46] However, reactive astrocytes can mediate neuroinflammation, leading to neuronal damage, and release some inflammatory factors that prevent myelin sheath regeneration.[47] Therefore, reduction of the extent of astrogliosis might be beneficial for neuronal development and remyelination. More importantly, we found that KD can inhibit the CPZ-induced activation of astrocytes and regulate the astroglial morphology, in order to return to normal conditions, suggesting that KD provides a supportive environment for neuronal growth and remyelination.

KD decreased the oxidative stress in the hippocampus of CPZ-fed mice

A former study demonstrated that CPZ intoxication increases oxidative stress, which in turn, triggers apoptosis in mature OLs.[48] This perturbation of biochemical redox state could lead to neuronal changes and cognitive impairment in CPZ-treated mice and inhibit remyelination.[16] In the present study, the GSH content and GSH-Px activity were nearly two-folds lower in CPZ+ND group, when compared to the ND group (Figures 8A and 8B, $P<0.001$). However, compared with the CPZ+ND group, the GSH content and GSH-PX activity were significantly increased in the KD+CPZ group (Figures 8A and 8B, $P<0.01$). In addition, as shown in Figure 8C, the concentration of MDA significantly higher in the CPZ+ND group than the ND group ($P<0.001$). However, the MDA content significantly decreased after KD treatment ($P<0.001$). Thus, our data suggest that KD inhibits oxidative stress in CPZ-fed mice.

SIRT1-expressing cells in the hippocampus

The double-staining with cellular markers revealed SIRT1 expression in $NG2^+$ OPCs (Figure 9A), $CNPase^+$ OLs (Figure 9B), Iba-1^+ microglia (Figure 9C), and $GFAP^+$ astrocytes (Figure 9D) in the hippocampus. We found that more of the SIRT1 deposits co-localized with $GFAP^+$ cells in the CPZ+KD, when compared to the CPZ+ND groups (Figure 9D). Some of the Iba-1^+ microglia and $CNPase^+$ OLs co-localized with SIRT1 staining (Figure 9C) in the ND, CPZ+ND and CPZ+KD groups. However few NG2 positive OPCs expressed SIRT1 in the ND, CPZ+ND and CPZ+KD groups (Figures 9A and 9B). The small images in the right-most column in Figure 9 present the magnification of the white-labeled region.

Effect of KD on the SIRT1/PPAR-γ/p-Akt/mTOR protein expression

SIRT1 activation plays a protective role in neurodegenerative diseases of mice, and acts as a potential treatment for neurodegeneration in MS.[49] A previous study revealed that the overexpression of SIRT1 protein exerts neuroprotective effects in EAE mice.[50] Our results revealed that the protein expression of SIRT1 decreased in the CPZ+ND group, while the level of SIRT1 significantly increased after KD treatment (Figures 10A and 10B, $P<0.001$). This indicates that KD promotes the expression of SIRT1, and ameliorates the demyelination in the experimental model. Furthermore, the PPAR-γ protein expression significantly decreased in the CPZ+ND group, when compared to the ND group. Interestingly, the KD treatment dramatically downregulated the level of PPAR-γ (Figures 10E and 10F, $P<0.001$). Furthermore, the *p*-Akt and mTOR protein expression levels were significantly higher in the CPZ+KD group compared to the CPZ+ND group (Figures 10A, 10C and 10D; $P<0.001$). Recent reports have shown that activating the *p*-Akt/mTOR signaling pathway enhances CNS myelination.[25,51] Thus, these present findings

suggest that KD may alleviate demyelination in the hippocampus by increasing the SIRT/PPAR-γ/*p*-Akt/mTOR protein expression.

Discussion

The present study investigated the effect of KD on demyelination in the hippocampus of mice during CPZ administration. We found that (1) KD could alleviate the demyelination in the hippocampus of CPZ-fed mice. (2) KD ameliorated the CPZ-induced learning and memory deficits. (3) KD promoted the OPCs differentiation and maturation. (4) KD suppressed the microglia activation and reactive astrocytes in the hippocampus of mice that received CPZ. (5) KD reduced the oxidative stress in the hippocampus of CPZ-fed mice. (6) KD increased the SIRT1, PPAR-γ, *p*-Akt and mTOR protein expression levels in the hippocampus.

In the present experiments, we found that the content of ketone bodies in blood and hippocampal β-hydroxybutyric acid significantly increased in the CPZ+KD group, while the blood glucose did not differ among groups (data not shown). These results indicate that the protective effect of KD in the hippocampus of mice during media with CPZ was partly due to the high levels of ketone bodies. Furthermore, in the present study, the ketosis effectively enhanced ketone body levels (3 mmol/L) in adult mice with KD treatment, suggesting that KD successfully induced the ketosis in the experiments.

CPZ induced behavioral and motor abnormalities, and cognitive deficits, as demonstrated by the OF, RT and MWM tests, which agrees with previous reports.[27,40] Motor dysfunction and behavioral disorders are correlated to the white matter damage caused by myelin loss, and may be correlated to the impaired regeneration ability of OLs and its progenitors.[52] The present results show that KD treatment improved motor functions, spontaneous exploration and spatial memory

406 learning of mice that received CPZ, indicating that KD treatment ameliorates the CPZ-induced
407 demyelination. Furthermore, H&E staining revealed that the nuclei of granule neurons in the
408 hippocampus became pyknotic after the animals received CPZ, while the KD treatment decreased
409 the damage to granule neurons in the DG areas of the hippocampus. Noteworthy, marked neuronal
410 changes were observed in CPZ+ND-treated mice with increased pyknotic neurons and less visible
411 Nissl bodies, while KD treatment reduced the damage to hippocampal neurons. This suggests that
412 KD plays a critical role in neuroprotection in hippocampal neurons of mice that received CPZ.
413 OPCs are located adjacent to the demyelinated lesions, and contributes to myelin repair. In the
414 present study, CPZ induced a significant increased in $NG2^+$ OPCs cells expression, which is in
415 agreement with previous reports.[53] However, treatment with KD resulted in the reduction of $NG2^+$
416 OPCs cells expression. In addition, we found that KD administration improved the expression of
417 MBP and upregulated the expression of CNPase in hippocampus of mice at day 35. These results
418 further confirm that KD promote the differentiation of OPCs and the survival of mature OLs.
419 Microglia activation plays an important role in demyelinating disorders. The classically
420 activated M1 type microglia can exacerbates neuronal damage and aggravates the severity of
421 demyelinating lesions.[54,55] In the present study, the number of $CD68^+$ and $CD16/32^+$ cells
422 significantly decreased in the CPZ+KD group compared with the CPZ+ND group. This suggests
423 that KD can inhibit the activation of microglia and M1-liked microglia polarization in the
424 hippocampus, which may generates an anti-inflammatory environment and promotes
425 remyelination.
426 Astrocytes, which is the important glial cells in CNS. It has been reported that reactive
427 astrocytes is harmful for axonal regeneration and remyelination.[56,57] Previous studies have

demonstrated that astrocyte ablation can improve the remyelination in the demyelination mouse model.[58] The present study has similar findings, in which the density of $GFAP^+$ cells significantly decreased at day 35 with KD administration. This suggests that the strategy of KD therapy in attenuating astrocyte activation is considered advantageous for myelin regeneration.

Oxidative stress is generally considered as a state of abundance of ROS.[59] Reducing oxidative stress in the EAE model has been reported to increase the density of OPCs and improve the remyelination in the CNS.[60] Ziegler et al. reported that KD exert a neuroprotective effect via reduction in oxidative stress.[61] Our results revealed that the GSH content and activity of GSH-Px significantly increased, while the MDA content decreased after KD administration in the hippocampus. Therefore, we suggest that KD acts against CPZ-induced demyelination in the hippocampus at least by increasing antioxidant activity.

The role of SIRT1 in inhibiting oxidative stress and demyelination has been described in a former study.[49] The present immunohistochemical stainings revealed that there was more SIRT1 expression in GFAP-positive astrocytes, some SIRT1 was co-expressed with Iba-1-positive microglia and CNPase-positive OLs, and few OPCs expressed SIRT1 in hippocampi of mice after KD feeding. In addition, there was more SIRT1 expression in GFAP-positive astrocytes in mice in the CPZ+KD group, when compared to the CPZ+ND group. It has been postulated that the neuroprotective roles of astrocytes with anti-inflammatory and anti-oxidative effects derive from the inhibition of the expression levels of IL-1β, and the increase in SOD2 enzyme activity via SIRT1 signaling activation.[62,63] Interestingly, we found that KD treatment significantly increased the SIRT1 expression of CPZ-fed mice. These results suggest that KD treatment has a neuroprotective effect against demyelination via increased expression of SIRT1.

In addition, SIRT1 and its numerous deacetylated substrates have been identified, such as PPAR-γ and PPAR-γ coactivator-1α.[64,65] A previous study demonstrated that docosahexaenoic acid might influence the process of OPCs maturation through its PPAR-γ agonistic activity.[66] Our results show that KD treatment increased the expression of PPAR-γ in the hippocampus, suggesting that KD can promote OPCs maturation in mice with CPZ-induced demyelination via the SIRT1/PPAR-γ signaling pathway. In addition, it has been reported that constitutively active p-Akt enhances the oligodendrocyte maturation in the CNS.[51] The histone deacetylase SIRT1 deacetylates Akt, and subsequently promotes the activation of Akt.[20,67] Earlier studies have confirmed that both SIRT1 and Akt play important roles in neuronal survival.[68,69] Moreover, it has been reported that the activation of the PI3K/p-Akt/mTOR signaling pathways can increase the number of OLs and enhance the remyelination in the EAE model.[70] MTOR works as the substrate of p-AKT in the downstream signaling pathway, it plays an important role in OPCs differentiation during development in the CNS. In the present study, CPZ intoxication significantly downregulated the protein expression of p-AKT and mTOR. However, KD treatment enhanced the p-AKT and mTOR protein expression levels. Therefore, these present results suggest that the activation of the SIRT1/*p*-AKT/mTOR pathway by KD plays a critical role in protecting against CPZ-induced demyelination.

Conclusion

In conclusion, these present results demonstrate that KD treatment exerts a protective effect in mice with CPZ-induced demyelination by improving spatial learning and memory, inhibiting the activation of astrocytes and microglia (especially the M1-like microglia), promoting OPC differentiation and maturation, and attenuating oxidative stress. Furthermore, KD plays a critical

472 role in protecting against CPZ-induced demyelination in the hippocampus by the SIRT1/PPAR-γ
473 pathway and SIRT1/*p*-Akt/mTOR pathway. These findings indicate that KD can be used as an
474 effective strategy to treat demyelinating diseases and ameliorate the clinical symptoms of MS.

475 **Acknowledgements** This work was supported by Open Project of Shandong Collaborative
476 Innovation Center for Antibody Drugs (No.CIC-AD1829 and No.CIC-AD1834), Doctoral
477 Foundation of Liaocheng University (No. 318051738 and No. 318051827), Foundation of
478 Liaocheng University (No.318011907)

479 **Conflicts of interest** The authors declare that they have no conflict of interest.

480 ## References

481 1. Zhang, N.; Liu, C.; Zhang, R.; Jin, L.; Yin, X.; Zheng, X.; Siebert, H. C.; Li, Y.; Wang, Z.; Loers, G.;
482 Petridis, A. K., Amelioration of clinical course and demyelination in the cuprizone mouse model in
483 relation to ketogenic diet. *Food Funct* **2020**.
484 2. Feng, X.; Bao, R.; Li, L.; Deisenhammer, F.; Arnason, B. G. W.; Reder, A. T., Interferon-beta
485 corrects massive gene dysregulation in multiple sclerosis: Short-term and long-term effects on
486 immune regulation and neuroprotection. *EBioMedicine* **2019**, *49*, 269-283.
487 3. Buesa-Estellez, A.; Cano-de-la-Cuerda, R.; Ortiz-Gutierrez, R. M.; Palacios-Cena, D., The impact of
488 pharmacological treatment on patients with multiple sclerosis. *Disabil Health J* **2019**, *12*, 615-621.
489 4. Lee, J. E.; Titcomb, T. J.; Bisht, B.; Rubenstein, L. M.; Louison, R.; Wahls, T. L., A Modified
490 MCT-Based Ketogenic Diet Increases Plasma beta-Hydroxybutyrate but Has Less Effect on Fatigue and
491 Quality of Life in People with Multiple Sclerosis Compared to a Modified Paleolithic Diet: A
492 Waitlist-Controlled, Randomized Pilot Study. *J Am Coll Nutr* **2020**, 1-13.
493 5. Bahr, L. S.; Bock, M.; Liebscher, D.; Bellmann-Strobl, J.; Franz, L.; Pruss, A.; Schumann, D.; Piper, S.
494 K.; Kessler, C. S.; Steckhan, N.; Michalsen, A.; Paul, F.; Mahler, A., Ketogenic diet and fasting diet as
495 Nutritional Approaches in Multiple Sclerosis (NAMS): protocol of a randomized controlled study. *Trials*
496 **2020**, *21*, 3.
497 6. Klement, R. J., Wilhelm Brunings' forgotten contribution to the metabolic treatment of cancer
498 utilizing hypoglycemia and a very low carbohydrate (ketogenic) diet. *J Tradit Complement Med* **2019**,
499 *9*, 192-200.
500 7. Storoni, M.; Plant, G. T., The Therapeutic Potential of the Ketogenic Diet in Treating Progressive
501 Multiple Sclerosis. *Mult Scler Int* **2015**, *2015*, 681289.
502 8. Nathan, J.; Khedekar Kale, D.; Naik, V. D.; Thakker, F.; Bailur, S., Dietary Therapy in Secondary
503 Progressive Multiple Sclerosis: A Case Report. *Cureus* **2019**, *11*, e5341.
504 9. Haindl, M. T.; Kock, U.; Zeitelhofer-Adzemovic, M.; Fazekas, F.; Hochmeister, S., The formation of
505 a glial scar does not prohibit remyelination in an animal model of multiple sclerosis. *Glia* **2019**, *67*,
506 467-481.

10. Olah, M.; Amor, S.; Brouwer, N.; Vinet, J.; Eggen, B.; Biber, K.; Boddeke, H. W., Identification of a microglia phenotype supportive of remyelination. *Glia* **2012**, *60*, 306-21.
11. Guo, M. F.; Meng, J.; Li, Y. H.; Yu, J. Z.; Liu, C. Y.; Feng, L.; Yang, W. F.; Li, J. L.; Feng, Q. J.; Xiao, B. G.; Ma, C. G., The inhibition of Rho kinase blocks cell migration and accumulation possibly by challenging inflammatory cytokines and chemokines on astrocytes. *J Neurol Sci* **2014**, *343*, 69-75.
12. Abe, H.; Saito, F.; Tanaka, T.; Mizukami, S.; Hasegawa-Baba, Y.; Imatanaka, N.; Akahori, Y.; Yoshida, T.; Shibutani, M., Developmental cuprizone exposure impairs oligodendrocyte lineages differentially in cortical and white matter tissues and suppresses glutamatergic neurogenesis signals and synaptic plasticity in the hippocampal dentate gyrus of rats. *Toxicol Appl Pharmacol* **2016**, *290*, 10-20.
13. van der Star, B. J.; Vogel, D. Y.; Kipp, M.; Puentes, F.; Baker, D.; Amor, S., In vitro and in vivo models of multiple sclerosis. *CNS Neurol Disord Drug Targets* **2012**, *11*, 570-88.
14. Clarner, T.; Janssen, K.; Nellessen, L.; Stangel, M.; Skripuletz, T.; Krauspe, B.; Hess, F. M.; Denecke, B.; Beutner, C.; Linnartz-Gerlach, B.; Neumann, H.; Vallieres, L.; Amor, S.; Ohl, K.; Tenbrock, K.; Beyer, C.; Kipp, M., CXCL10 triggers early microglial activation in the cuprizone model. *J Immunol* **2015**, *194*, 3400-13.
15. Blakemore, W. F., Observations on oligodendrocyte degeneration, the resolution of status spongiosus and remyelination in cuprizone intoxication in mice. *J Neurocytol* **1972**, *1*, 413-26.
16. Omotoso, G. O.; Olajide, O. J.; Gbadamosi, I. T.; Adebayo, J. O.; Enaibe, B. U.; Akinola, O. B.; Owoyele, B. V., Cuprizone toxicity and Garcinia kola biflavonoid complex activity on hippocampal morphology and neurobehaviour. *Heliyon* **2019**, *5*, e02102.
17. Kim, D. Y.; Hao, J.; Liu, R.; Turner, G.; Shi, F. D.; Rho, J. M., Inflammation-mediated memory dysfunction and effects of a ketogenic diet in a murine model of multiple sclerosis. *PLoS One* **2012**, *7*, e35476.
18. Jeong, H.; Cohen, D. E.; Cui, L.; Supinski, A.; Savas, J. N.; Mazzulli, J. R.; Yates, J. R., 3rd; Bordone, L.; Guarente, L.; Krainc, D., Sirt1 mediates neuroprotection from mutant huntingtin by activation of the TORC1 and CREB transcriptional pathway. *Nat Med* **2011**, *18*, 159-65.
19. Jiang, M.; Wang, J.; Fu, J.; Du, L.; Jeong, H.; West, T.; Xiang, L.; Peng, Q.; Hou, Z.; Cai, H.; Seredenina, T.; Arbez, N.; Zhu, S.; Sommers, K.; Qian, J.; Zhang, J.; Mori, S.; Yang, X. W.; Tamashiro, K. L.; Aja, S.; Moran, T. H.; Luthi-Carter, R.; Martin, B.; Maudsley, S.; Mattson, M. P.; Cichewicz, R. H.; Ross, C. A.; Holtzman, D. M.; Krainc, D.; Duan, W., Neuroprotective role of Sirt1 in mammalian models of Huntington's disease through activation of multiple Sirt1 targets. *Nat Med* **2011**, *18*, 153-8.
20. Sundaresan, N. R.; Pillai, V. B.; Wolfgeher, D.; Samant, S.; Vasudevan, P.; Parekh, V.; Raghuraman, H.; Cunningham, J. M.; Gupta, M.; Gupta, M. P., The deacetylase SIRT1 promotes membrane localization and activation of Akt and PDK1 during tumorigenesis and cardiac hypertrophy. *Sci Signal* **2011**, *4*, ra46.
21. Li, Q.; Peng, Y.; Fan, L.; Xu, H.; He, P.; Cao, S.; Li, J.; Chen, T.; Ruan, W.; Chen, G., Phosphodiesterase-4 inhibition confers a neuroprotective efficacy against early brain injury following experimental subarachnoid hemorrhage in rats by attenuating neuronal apoptosis through the SIRT1/Akt pathway. *Biomed Pharmacother* **2018**, *99*, 947-955.
22. Shin, J. A.; Lee, K. E.; Kim, H. S.; Park, E. M., Acute resveratrol treatment modulates multiple signaling pathways in the ischemic brain. *Neurochem Res* **2012**, *37*, 2686-96.
23. Kumar, S.; Patel, R.; Moore, S.; Crawford, D. K.; Suwanna, N.; Mangiardi, M.; Tiwari-Woodruff, S. K., Estrogen receptor beta ligand therapy activates PI3K/Akt/mTOR signaling in oligodendrocytes and

promotes remyelination in a mouse model of multiple sclerosis. *Neurobiol Dis* **2013**, *56*, 131-44.
24. Narayanan, S. P.; Flores, A. I.; Wang, F.; Macklin, W. B., Akt signals through the mammalian target of rapamycin pathway to regulate CNS myelination. *J Neurosci* **2009**, *29*, 6860-70.
25. Bernardo, A.; Bianchi, D.; Magnaghi, V.; Minghetti, L., Peroxisome proliferator-activated receptor-gamma agonists promote differentiation and antioxidant defenses of oligodendrocyte progenitor cells. *J Neuropathol Exp Neurol* **2009**, *68*, 797-808.
26. Hao, G. W.; Chen, Y. S.; He, D. M.; Wang, H. Y.; Wu, G. H.; Zhang, B., Growth of human colon cancer cells in nude mice is delayed by ketogenic diet with or without omega-3 fatty acids and medium-chain triglycerides. *Asian Pac J Cancer Prev* **2015**, *16*, 2061-8.
27. Zhang, Y.; Bi, X.; Adebiyi, O.; Wang, J.; Mooshekhian, A.; Cohen, J.; Wei, Z.; Wang, F.; Li, X. M., Venlafaxine Improves the Cognitive Impairment and Depression-Like Behaviors in a Cuprizone Mouse Model by Alleviating Demyelination and Neuroinflammation in the Brain. *Front Pharmacol* **2019**, *10*, 332.
28. Janssen, C. I.; Zerbi, V.; Mutsaers, M. P.; de Jong, B. S.; Wiesmann, M.; Arnoldussen, I. A.; Geenen, B.; Heerschap, A.; Muskiet, F. A.; Jouni, Z. E.; van Tol, E. A.; Gross, G.; Homberg, J. R.; Berg, B. M.; Kiliaan, A. J., Impact of dietary n-3 polyunsaturated fatty acids on cognition, motor skills and hippocampal neurogenesis in developing C57BL/6J mice. *J Nutr Biochem* **2015**, *26*, 24-35.
29. Wang, W.; Liu, L.; Jiang, P.; Chen, C.; Zhang, T., Levodopa improves learning and memory ability on global cerebral ischemia-reperfusion injured rats in the Morris water maze test. *Neurosci Lett* **2017**, *636*, 233-240.
30. Lindner, M.; Heine, S.; Haastert, K.; Garde, N.; Fokuhl, J.; Linsmeier, F.; Grothe, C.; Baumgartner, W.; Stangel, M., Sequential myelin protein expression during remyelination reveals fast and efficient repair after central nervous system demyelination. *Neuropathol Appl Neurobiol* **2008**, *34*, 105-14.
31. Wang, X.; Wu, X.; Liu, Q.; Kong, G.; Zhou, J.; Jiang, J.; Wu, X.; Huang, Z.; Su, W.; Zhu, Q., Ketogenic Metabolism Inhibits Histone Deacetylase (HDAC) and Reduces Oxidative Stress After Spinal Cord Injury in Rats. *Neuroscience* **2017**, *366*, 36-43.
32. Yang, L.; Sun, Y. Y.; Liu, Y. R.; Yin, N. N.; Bu, F. T.; Yu, H. X.; Du, X. S.; Li, J.; Huang, C., PTP1B promotes macrophage activation by regulating the NF-kappaB pathway in alcoholic liver injury. *Toxicol Lett* **2020**, *319*, 11-21.
33. Jang, M. S.; Oh, S. K.; Lee, S. W.; Jeong, S. H.; Kim, H., Moderate brain hypothermia started before resuscitation improves survival and neurobehavioral outcomes after CA/CPR in mice. *Am J Emerg Med* **2019**, *37*, 1942-1948.
34. Qin, S.; Sun, D.; Zhang, C.; Tang, Y.; Zhou, F.; Zheng, K.; Tang, R.; Zheng, Y., Downregulation of sonic hedgehog signaling in the hippocampus leads to neuronal apoptosis in high-fat diet-fed mice. *Behav Brain Res* **2019**, *367*, 91-100.
35. Hoffmann, K.; Lindner, M.; Groticke, I.; Stangel, M.; Loscher, W., Epileptic seizures and hippocampal damage after cuprizone-induced demyelination in C57BL/6 mice. *Exp Neurol* **2008**, *210*, 308-21.
36. Koutsoudaki, P. N.; Skripuletz, T.; Gudi, V.; Moharregh-Khiabani, D.; Hildebrandt, H.; Trebst, C.; Stangel, M., Demyelination of the hippocampus is prominent in the cuprizone model. *Neurosci Lett* **2009**, *451*, 83-8.
37. Zhang, Z.; Li, D.; Xu, L.; Li, H. P., Sirt1 improves functional recovery by regulating autophagy of astrocyte and neuron after brain injury. *Brain Res Bull* **2019**, *150*, 42-49.
38. Li, Z.; He, Y.; Fan, S.; Sun, B., Clemastine rescues behavioral changes and enhances remyelination

595 in the cuprizone mouse model of demyelination. *Neurosci Bull* **2015**, *31*, 617-25.
596 39. Yu, H.; Wu, M.; Lu, G.; Cao, T.; Chen, N.; Zhang, Y.; Jiang, Z.; Fan, H.; Yao, R., Prednisone alleviates
597 demyelination through regulation of the NLRP3 inflammasome in a C57BL/6 mouse model of
598 cuprizone-induced demyelination. *Brain Res* **2018**, *1678*, 75-84.
599 40. Liu, J.; Tian, D.; Murugan, M.; Eyo, U. B.; Dreyfus, C. F.; Wang, W.; Wu, L. J., Microglial Hv1 proton
600 channel promotes cuprizone-induced demyelination through oxidative damage. *J Neurochem* **2015**,
601 *135*, 347-56.
602 41. Wegner, C.; Esiri, M. M.; Chance, S. A.; Palace, J.; Matthews, P. M., Neocortical neuronal,
603 synaptic, and glial loss in multiple sclerosis. *Neurology* **2006**, *67*, 960-7.
604 42. Aryanpour, R.; Pasbakhsh, P.; Zibara, K.; Namjoo, Z.; Beigi Boroujeni, F.; Shahbeigi, S.; Kashani, I.
605 R.; Beyer, C.; Zendehdel, A., Progesterone therapy induces an M1 to M2 switch in microglia
606 phenotype and suppresses NLRP3 inflammasome in a cuprizone-induced demyelination mouse model.
607 *Int Immunopharmacol* **2017**, *51*, 131-139.
608 43. Gudi, V.; Moharregh-Khiabani, D.; Skripuletz, T.; Koutsoudaki, P. N.; Kotsiari, A.; Skuljec, J.; Trebst,
609 C.; Stangel, M., Regional differences between grey and white matter in cuprizone induced
610 demyelination. *Brain Res* **2009**, *1283*, 127-38.
611 44. Li, T.; Niu, J.; Yu, G.; Ezan, P.; Yi, C.; Wang, X.; Koulakoff, A.; Gao, X.; Chen, X.; Saez, J. C.; Giaume,
612 C.; Xiao, L., Connexin 43 deletion in astrocytes promotes CNS remyelination by modulating local
613 inflammation. *Glia* **2020**, *68*, 1201-1212.
614 45. Ledoux, S. P.; Shen, C. C.; Grishko, V. I.; Fields, P. A.; Gard, A. L.; Wilson, G. L., Glial cell-specific
615 differences in response to alkylation damage. *Glia* **1998**, *24*, 304-12.
616 46. Giulian, D., Reactive glia as rivals in regulating neuronal survival. *Glia* **1993**, *7*, 102-10.
617 47. Cervos-Navarro, J.; Lafuente, J. V., Traumatic brain injuries: structural changes. *J Neurol Sci* **1991**,
618 *103 Suppl*, S3-14.
619 48. Praet, J.; Guglielmetti, C.; Berneman, Z.; Van der Linden, A.; Ponsaerts, P., Cellular and molecular
620 neuropathology of the cuprizone mouse model: clinical relevance for multiple sclerosis. *Neurosci*
621 *Biobehav Rev* **2014**, *47*, 485-505.
622 49. Martin, A.; Tegla, C. A.; Cudrici, C. D.; Kruszewski, A. M.; Azimzadeh, P.; Boodhoo, D.; Mekala, A.
623 P.; Rus, V.; Rus, H., Role of SIRT1 in autoimmune demyelination and neurodegeneration. *Immunol Res*
624 **2015**, *61*, 187-97.
625 50. Wang, J.; Zhao, C.; Kong, P.; Bian, G.; Sun, Z.; Sun, Y.; Guo, L.; Li, B., Methylene blue alleviates
626 experimental autoimmune encephalomyelitis by modulating AMPK/SIRT1 signaling pathway and
627 Th17/Treg immune response. *J Neuroimmunol* **2016**, *299*, 45-52.
628 51. Flores, A. I.; Narayanan, S. P.; Morse, E. N.; Shick, H. E.; Yin, X.; Kidd, G.; Avila, R. L.; Kirschner, D.
629 A.; Macklin, W. B., Constitutively active Akt induces enhanced myelination in the CNS. *J Neurosci* **2008**,
630 *28*, 7174-83.
631 52. Tomlinson, L.; Leiton, C. V.; Colognato, H., Behavioral experiences as drivers of oligodendrocyte
632 lineage dynamics and myelin plasticity. *Neuropharmacology* **2016**, *110*, 548-562.
633 53. VonDran, M. W.; Singh, H.; Honeywell, J. Z.; Dreyfus, C. F., Levels of BDNF impact
634 oligodendrocyte lineage cells following a cuprizone lesion. *J Neurosci* **2011**, *31*, 14182-90.
635 54. Gerhauser, I.; Hansmann, F.; Puff, C.; Kumnok, J.; Schaudien, D.; Wewetzer, K.; Baumgartner, W.,
636 Theiler's murine encephalomyelitis virus induced phenotype switch of microglia in vitro. *J*
637 *Neuroimmunol* **2012**, *252*, 49-55.
638 55. Hansmann, F.; Zhang, N.; Herder, V.; Leitzen, E.; Baumgartner, W., Delayed Astrogliosis

Associated with Reduced M1 Microglia Activation in Matrix Metalloproteinase 12 Knockout Mice during Theiler's Murine Encephalomyelitis. *Int J Mol Sci* **2019**, *20*.

56. Gankam Kengne, F.; Nicaise, C.; Soupart, A.; Boom, A.; Schiettecatte, J.; Pochet, R.; Brion, J. P.; Decaux, G., Astrocytes are an early target in osmotic demyelination syndrome. *J Am Soc Nephrol* **2011**, *22*, 1834-45.

57. Sica, R. E.; Caccuri, R.; Quarracino, C.; Capani, F., Are astrocytes executive cells within the central nervous system? *Arq Neuropsiquiatr* **2016**, *74*, 671-8.

58. Madadi, S.; Pasbakhsh, P.; Tahmasebi, F.; Mortezaee, K.; Khanehzad, M.; Boroujeni, F. B.; Noorzehi, G.; Kashani, I. R., Astrocyte ablation induced by La-aminoadipate (L-AAA) potentiates remyelination in a cuprizone demyelinating mouse model. *Metab Brain Dis* **2019**, *34*, 593-603.

59. Islam, M. T., Oxidative stress and mitochondrial dysfunction-linked neurodegenerative disorders. *Neurol Res* **2017**, *39*, 73-82.

60. Mohajeri, M.; Sadeghizadeh, M.; Najafi, F.; Javan, M., Polymerized nano-curcumin attenuates neurological symptoms in EAE model of multiple sclerosis through down regulation of inflammatory and oxidative processes and enhancing neuroprotection and myelin repair. *Neuropharmacology* **2015**, *99*, 156-67.

61. Ziegler, D. R.; Ribeiro, L. C.; Hagenn, M.; Siqueira, I. R.; Araujo, E.; Torres, I. L.; Gottfried, C.; Netto, C. A.; Goncalves, C. A., Ketogenic diet increases glutathione peroxidase activity in rat hippocampus. *Neurochem Res* **2003**, *28*, 1793-7.

62. Cheng, Y.; Takeuchi, H.; Sonobe, Y.; Jin, S.; Wang, Y.; Horiuchi, H.; Parajuli, B.; Kawanokuchi, J.; Mizuno, T.; Suzumura, A., Sirtuin 1 attenuates oxidative stress via upregulation of superoxide dismutase 2 and catalase in astrocytes. *J Neuroimmunol* **2014**, *269*, 38-43.

63. Li, D.; Liu, N.; Zhao, H. H.; Zhang, X.; Kawano, H.; Liu, L.; Zhao, L.; Li, H. P., Interactions between Sirt1 and MAPKs regulate astrocyte activation induced by brain injury in vitro and in vivo. *J Neuroinflammation* **2017**, *14*, 67.

64. Herskovits, A. Z.; Guarente, L., SIRT1 in neurodevelopment and brain senescence. *Neuron* **2014**, *81*, 471-83.

65. Hwang, J. W.; Yao, H.; Caito, S.; Sundar, I. K.; Rahman, I., Redox regulation of SIRT1 in inflammation and cellular senescence. *Free Radic Biol Med* **2013**, *61*, 95-110.

66. Antonietta Ajmone-Cat, M.; Lavinia Salvatori, M.; De Simone, R.; Mancini, M.; Biagioni, S.; Bernardo, A.; Cacci, E.; Minghetti, L., Docosahexaenoic acid modulates inflammatory and antineurogenic functions of activated microglial cells. *J Neurosci Res* **2012**, *90*, 575-87.

67. Iaconelli, J.; Lalonde, J.; Watmuff, B.; Liu, B.; Mazitschek, R.; Haggarty, S. J.; Karmacharya, R., Lysine Deacetylation by HDAC6 Regulates the Kinase Activity of AKT in Human Neural Progenitor Cells. *ACS Chem Biol* **2017**, *12*, 2139-2148.

68. Zhang, X. S.; Wu, Q.; Wu, L. Y.; Ye, Z. N.; Jiang, T. W.; Li, W.; Zhuang, Z.; Zhou, M. L.; Zhang, X.; Hang, C. H., Sirtuin 1 activation protects against early brain injury after experimental subarachnoid hemorrhage in rats. *Cell Death Dis* **2016**, *7*, e2416.

69. Dai, Y.; Zhang, W.; Zhou, X.; Shi, J., Activation of the Protein Kinase B (Akt) Reduces Nur77-induced Apoptosis During Early Brain Injury after Experimental Subarachnoid Hemorrhage in Rat. *Ann Clin Lab Sci* **2015**, *45*, 615-22.

70. Liu, S. Q.; Zhang, M. L.; Zhang, H. J.; Liu, F. Z.; Chu, R. J.; Zhang, G. X.; Zhu, L., Matrine promotes oligodendrocyte development in CNS autoimmunity through the PI3K/Akt signaling pathway. *Life Sci* **2017**, *180*, 36-41.

FIGURE CAPTIONS

Figure 1 Effect of KD on body weight changes of mice. The body weight of mice was measured every two days during the experiment. The data are presented as mean ± standard error of the mean (SEM).The significant effects between groups are indicated by asterisks ($^{*}P<0.05$, $^{***}P<0.001$), n=8.

Figure 2 Behavioral test. (A) The representative images show the exploratory behavior of mice in the ND, CPZ+ND and CPZ+KD groups. (B) The total traveled distance. (C) The central distance traveled in the OF. (D) The time spent in the center area. (E) The average latency of mice to fall from the rotarod. KD treated mice had a significantly longer latency to fall, when compared to CPZ-alone treated mice, at five weeks post-induction. (F) Mouse trajectory during the probe trial. (G) Distance to target. (H) The number of platform crossings. (I) The time spent in the target quadrant. The green colored circle represents the starting point, while the red colored circle represents the terminal point. The date are presented as mean ± SEM (n=8). The green colored circle represents the starting point, while the red color circle represents the terminal point. The significant differences between ND groups are indicated: $^{***}P<0.001$. The significant differences between the CPZ+ND groups are indicated: $^{###}P<0.001$.

Figure 3 The concentration of β-hydroxybutyrate acid and the blood biochemical index were determined in mice with KD/ND treatment. (A) Mice in the CPZ+KD groups had significantly elevated concentration of blood ketone body, when compared to mice in the ND and CPZ+ND groups (n=8). (B) KD-treated mice had a significantly elevated concentration of β-hydroxybutyrate in hippocampus, when compared to ND-treated mice (n=4). (C-F) The ALT (C), AST (D), BUN (E) and Cr (F) of mice were determined after five weeks CPZ feeding with

KD/ND (n=8). The data were presented as mean ± SEM. The significant differences between ND groups are indicated: $^{***}P<0.001$. The significant differences between CPZ+ND groups are indicated: $^{###}P<0.001$.

Figure 4 Effect of KD on the myelination process in mice that received CPZ. The representative images show the MBP-stained coronal sections of the hippocampus in the ND group (A), CPZ+ND group (B) and CPZ+KD group (C) after five weeks post-induction. Scale bars = 200 μm. The black boxes represent the marked area in the hippocampus, as follows: black box 1 (A1, B1 and C1) represents the CA1 region, black box 2 (A2, B2 and C2) represents CA3 region, and black box 3 (A3, B3 and C3) represents the DG. Scale bars = 100 μm. (D) The immunohistochemistry for NG2 after five weeks of CPZ feeding in mice. Scale bars = 200 μm. (E-F) Quantitative analysis of the MBP immunodensity (E) and the number of $NG2^+$ cells (F) in the hippocampus in mice in each group. (G) Detection of the protein levels of CNPase in the hippocampus in the ND, CPZ+ND and CPZ+KD groups; β-actin was used as an internal control for normalization. (H) The quantitative analysis of CNPase levels was performed by western blot in the ND, CPZ+ND and CPZ+KD groups. The data are presented as mean ± SEM (n=4). The significant differences between ND groups are indicated: $^{*}P<0.05$, $^{***}P<0.001$. The significant differences between CPZ+ND groups are indicated: $^{#}P<0.05$, $^{###}P<0.001$.

Figure 5 Histological images of the hippocampus. (A) H&E staining of the hippocampus of mice in the ND, CPZ+ND and CPZ+KD groups at day 35. Scale bars = 200 μm. (B) H&E staining of the DG area of the hippocampus, and the black arrows point to pyknotic cells, Figure 5B is the partial enlargement of Figure 5A. (C) Nissl staining of the DG in the hippocampus at day 35. Scale bars = 100 μm.

Figure 6 The immunohistochemistry for the microglia in the hippocampus at day 35 after induction. (A-B) The representative brain sections stained for $CD68^+$ cells (A) and $CD16/32^+$ cells (B) are shown in the hippocampus in the ND, CPZ+ND and CPZ+KD groups. (C-D) Quantitative analysis of the number of $CD68^+$ cells (C) and $CD16/32^+$ cells (D) in the hippocampus in each group. The data are presented as mean ± SEM (n=4). Scale bars = 200 μm. The significant differences between ND groups are indicated as $^{*}P<0.05$, $^{***}P<0.001$. The significant differences between CPZ+ND groups are indicated as $^{###}P<0.001$.

Figure 7 GFAP immunohistochemistry staining in the hippocampus of mice. (A) The representative brain sections stained for GFAP are shown in the hippocampus of mice in the ND, CPZ+ND and CPZ+KD groups. Scale bars = 200 μm. (B) The morphological differences of GFAP-stained cells among the different groups. The magnification of the black-labeled box in Figure A, which marked the CA3 region of the hippocampus. Scale bars = 20 μm. (C) Quantitative analysis of the number of $GFAP^+$ cells in the hippocampus of mice in each group. The data are presented as mean ± SEM (n=4). The significant differences between ND groups are indicated: $^{***}P<0.001$. The significant differences between CPZ+ND groups are indicated: $^{###}P<0.001$.

Figure 8 Oxidative stress was assessed by detecting the GSH levels, GSH-Px activity and MDA content. (A-C) The GSH levels (A), GSH-Px activity (B) and MDA content (C) of the hippocampus were measured at day 35, after mice received CPZ. The data were presented as mean ± SEM (n=4). The significant differences between ND groups are indicated: $^{*}P<0.05$, $^{***}P<0.001$. The significant differences between CPZ+ND groups are indicated: $^{##}P<0.01$, $^{###}P<0.001$.

Figure 9 The immunofluorescence double-staining for SIRT1 with NG2, CNPase, Iba-1 and GFAP. The SIRT1 protein expression of OPCs, OLs, microglia and astrocytes in the CA1 region of the hippocampus at 35 days post-induction. SIRT1 (green) was expressed by OPCs (red, A), OLs (red, B), microglias (red, C) and astrocytes (red, D), as demonstrated by the orange-yellow mixed color. The nuclei were stained with DAPI. Scale bars = 50 μm.

Figure 10 KD promotes the protein expression of SIRT1, *p*-Akt, mTOR and PPAR-γ in the CPZ-induced model. (A) Representative examples of the western blot analysis, demonstrating the expression levels of SIRT1, *p*-Akt, mTOR and PPAR-γ in the hippocampus at day 35, and β-actin was used as an internal control for normalization. (B-D) Quantitative analysis of the SIRT1 level (B), *p*-Akt level (C) and mTOR level (D) by western blot in the ND, CPZ+ND and CPZ+KD groups. (E) Representative western blot images of PPAR-γ in the hippocampus at day 35, and GAPDH was used as an internal control for normalization. (F) Quantitative analysis of the PPAR-γ level by western blot in the ND, CPZ+ND and CPZ+KD groups. The data are presented as mean ± SEM (n=4). The significant differences between ND groups are indicated: **P<0.01, ***P<0.001. The significant differences between CPZ+ND groups are indicated: $^{\#}$P<0.05, $^{\#\#\#}$P<0.001.

Graphical abstract

Table 1. Composition of the ND and KD used in the present experiment

	ND		KD	
	Weight (grams/kg)	Energy density (kcal/g)	Weight (grams/kg)	Energy density (kcal/g)
Casein	200.000	0.800	194.000	0.776
Sucrose	132.000	0.528	/	/
Maltodextrin	100.000	0.400	/	/
Corn starch	397.500	1.590	/	/
L-Cystine	3.000	0.012	3.000	0.012
Cellulose	50.000	/	23.500	/
V1002 vitamin mix[a]	10.000	0.040	10.000	0.040
M1003G mineral mix	35.000	/	35.000	/
Choline bitartrate	2.500	/	2.500	/
Tert-butyl-hydroquinone	0.014	/	0.014	/
Soybean oil	70.000	0.630	85.000	0.765
MCT oil	/	/	370.000	3.330
MCT powder[b]	/	/	277.000	1.830
Total (gram)	1000.014	4.000	1000.014	6.753
Ketogenic ratio	0.080:1		3.060:1	

[a] Containing 100 % (w/w) sucrose.

[b] Containing 72 % (w/w) fat, 2.2 % (w/w) protein, 1.2 % (w/w) sucrose, 22.2 % (w/w) cellulose.

Table 2. Primary antibodies in the experiments

Protein	Primary Antibodies	Manufacturers	Dilution ratio
Astrocytes	anti-GFAP rabbit polyclonal antibody	Dako	1:200
Myelin proteolipid protein		Cytomation	1:1,000
Microglia/macrophage	anti-MBP rabbit polyclonal antibody	Millipore	1:600
M1 microglia	anti-CD68 rabbit polyclonal antibody	Abcam	1:600
OPCs	anti-CD16/32 rabbit polyclonal antibody	Abcam Chemicon	1:200
	anti-NG2 rabbit polyclonal antibody		

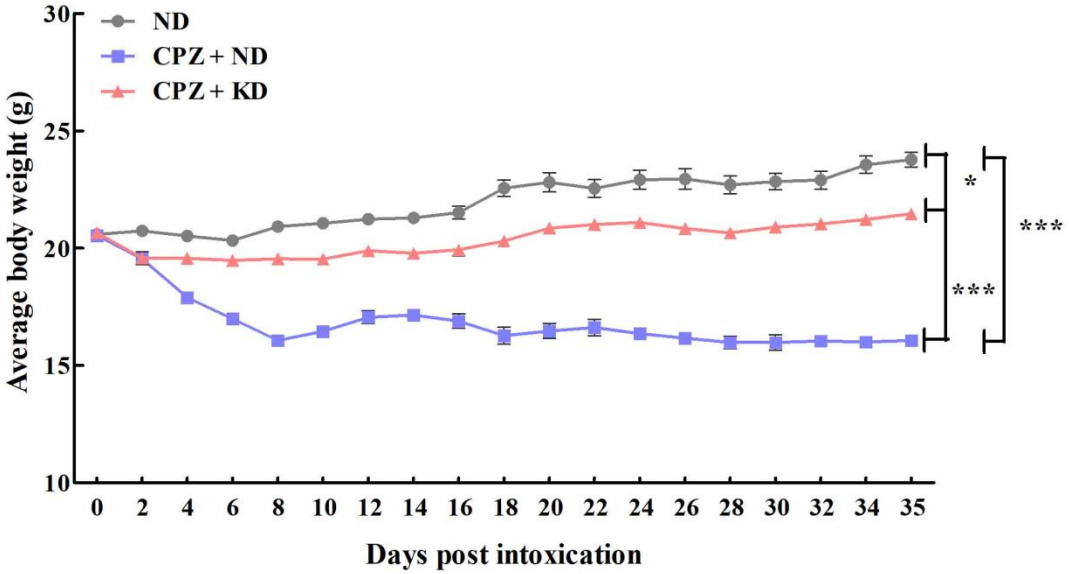
ND
CPZ + ND
CPZ + KD
Average body weight (g)
30
25
20
15
10
0 2 4 6 8 10 12 14 16 18 20 22 24 26 28 30 32 34 35
Days post intoxication
*
***
***

Figure 1

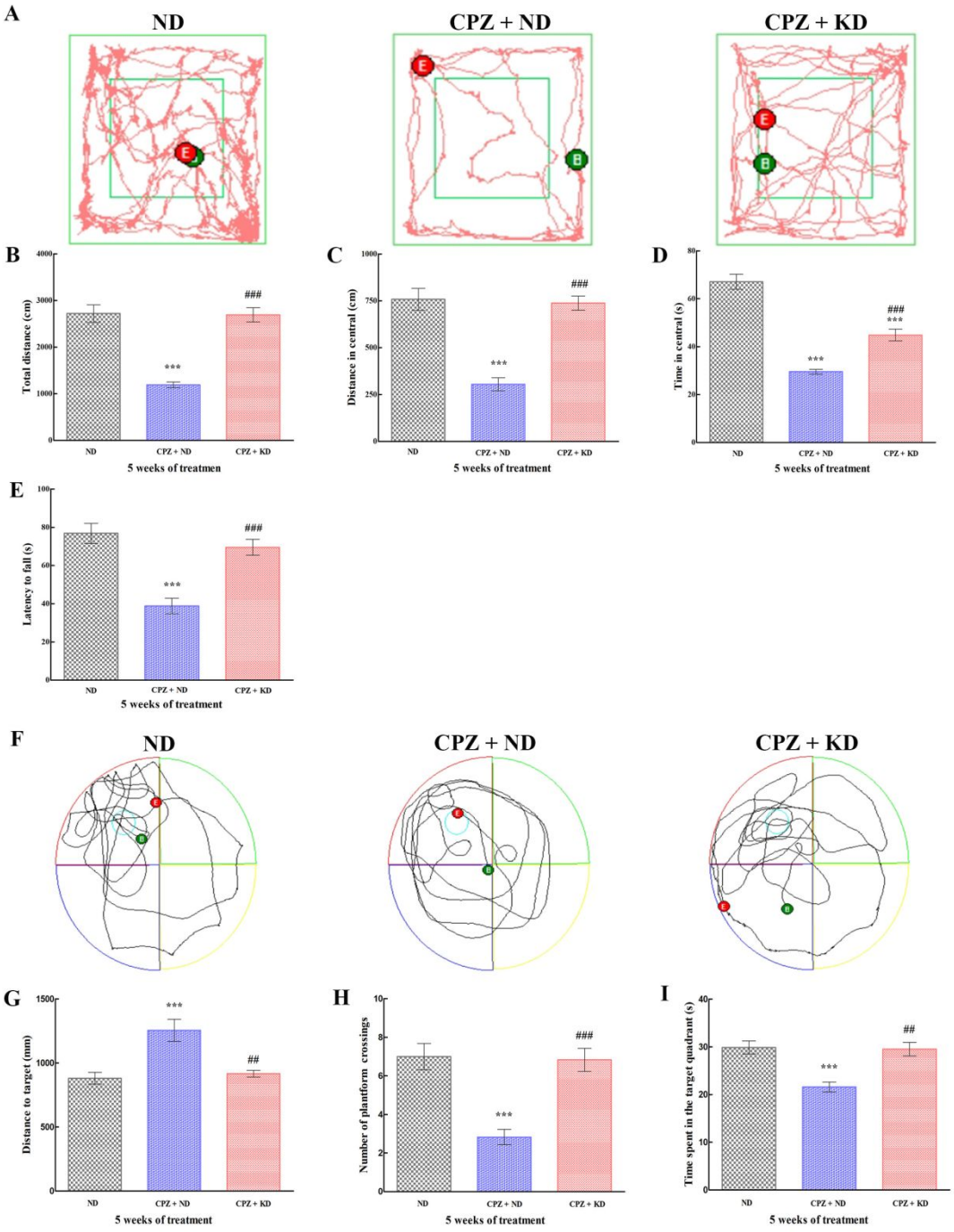
A
ND
CPZ + ND
CPZ + KD
B
Total distance (cm)
C
Distance in central (cm)
D
Time in central (s)
E
Latency to fall (s)
5 weeks of treatmen
5 weeks of treatment
F
ND
CPZ + ND
CPZ + KD
G
Distance to target (mm)
H
Number of plantform crossings
I
Time spent in the target quadrant (s)
ND
CPZ + ND
CPZ + KD

Figure 2

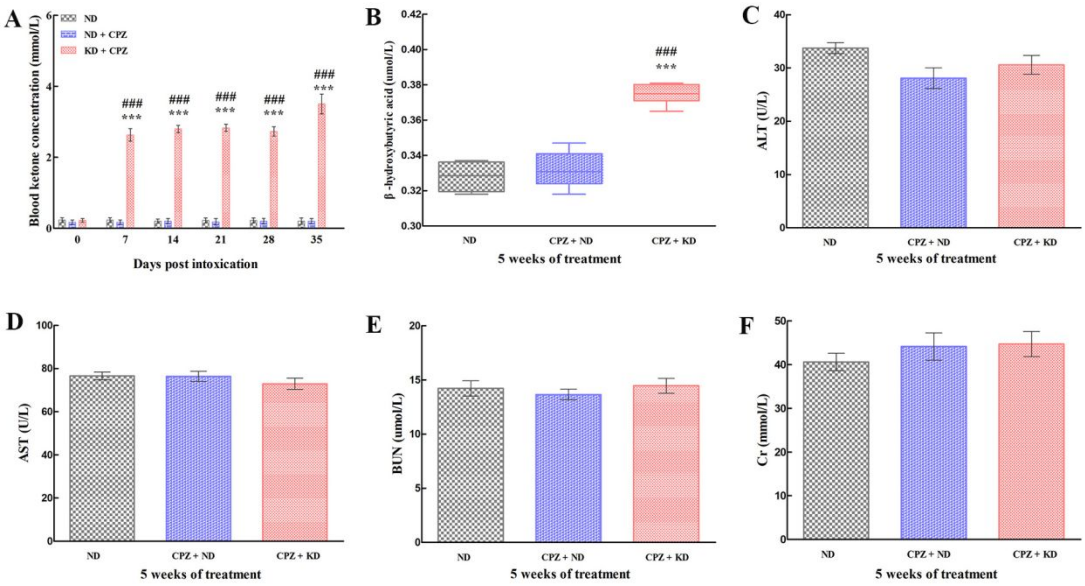
A
ND
ND + CPZ
KD + CPZ
Blood ketone concentration (mmol/L)
Days post intoxication
B
β -hydroxybutyric acid (umol/L)
5 weeks of treatment
C
ALT (U/L)
5 weeks of treatment
D
AST (U/L)
5 weeks of treatment
E
BUN (umol/L)
5 weeks of treatment
F
Cr (mmol/L)
5 weeks of treatment

Figure 3

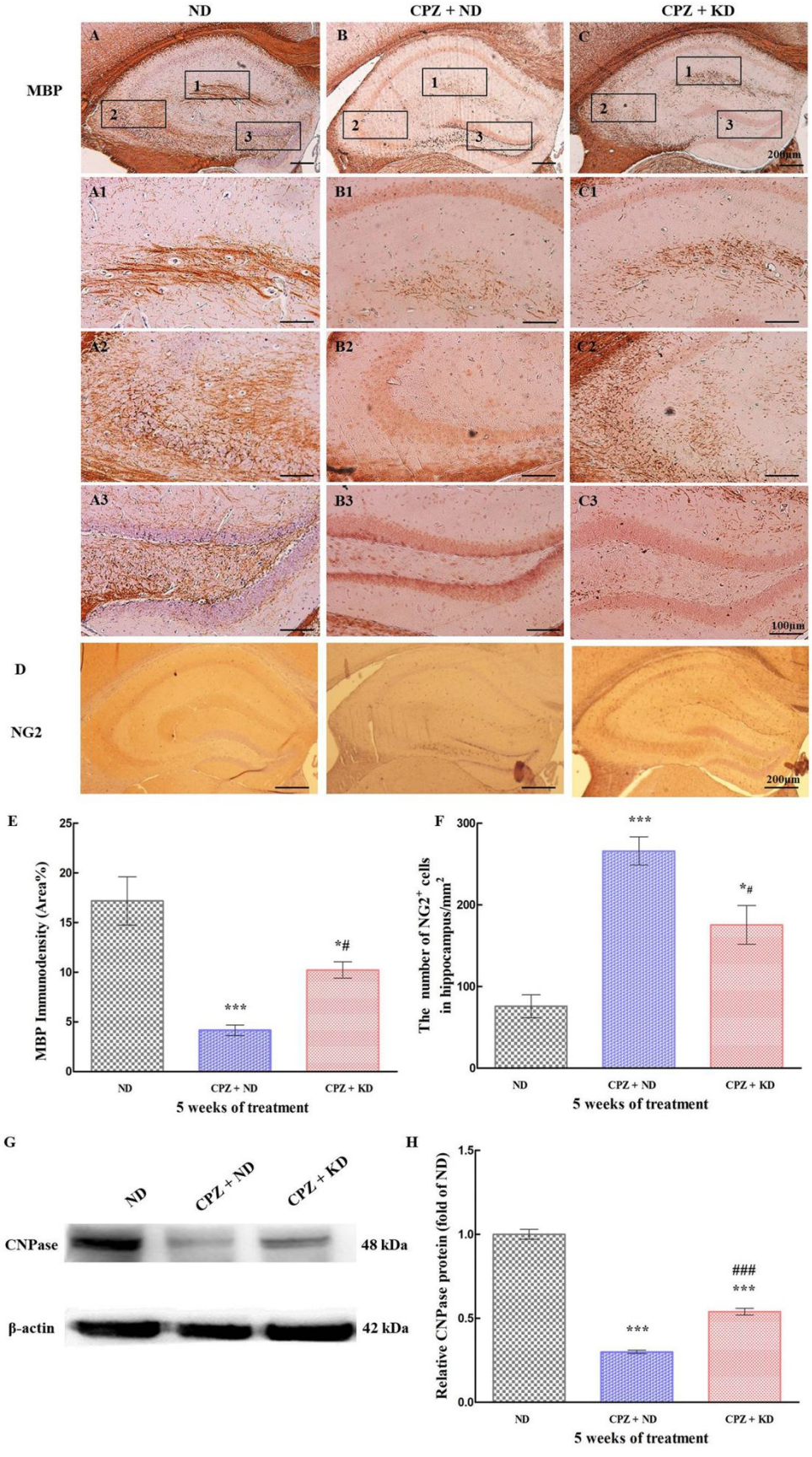
ND
CPZ + ND
CPZ + KD
MBP
A
B
C
1
2
3
200μm
A1
B1
C1
A2
B2
C2
A3
B3
C3
100μm
D
NG2
200μm
E
MBP Immunodensity (Area%)
25
20
15
10
5
0
***
*#
ND
CPZ + ND
CPZ + KD
5 weeks of treatment
F
The number of NG2+ cells in hippocampus/mm2
300
200
100
0
***
*#
ND
CPZ + ND
CPZ + KD
5 weeks of treatment
G
ND
CPZ + ND
CPZ + KD
CNPase
48 kDa
β-actin
42 kDa
H
Relative CNPase protein (fold of ND)
1.5
1.0
0.5
0.0
###
***
***
ND
CPZ + ND
CPZ + KD
5 weeks of treatment

Figure 4

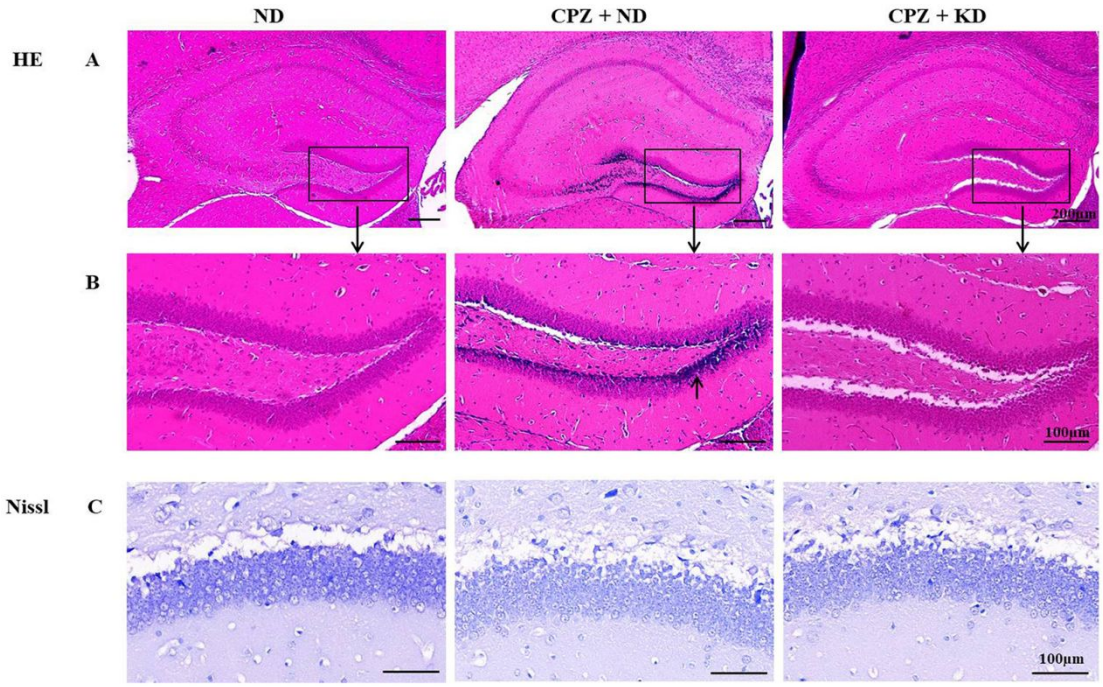

Figure 5

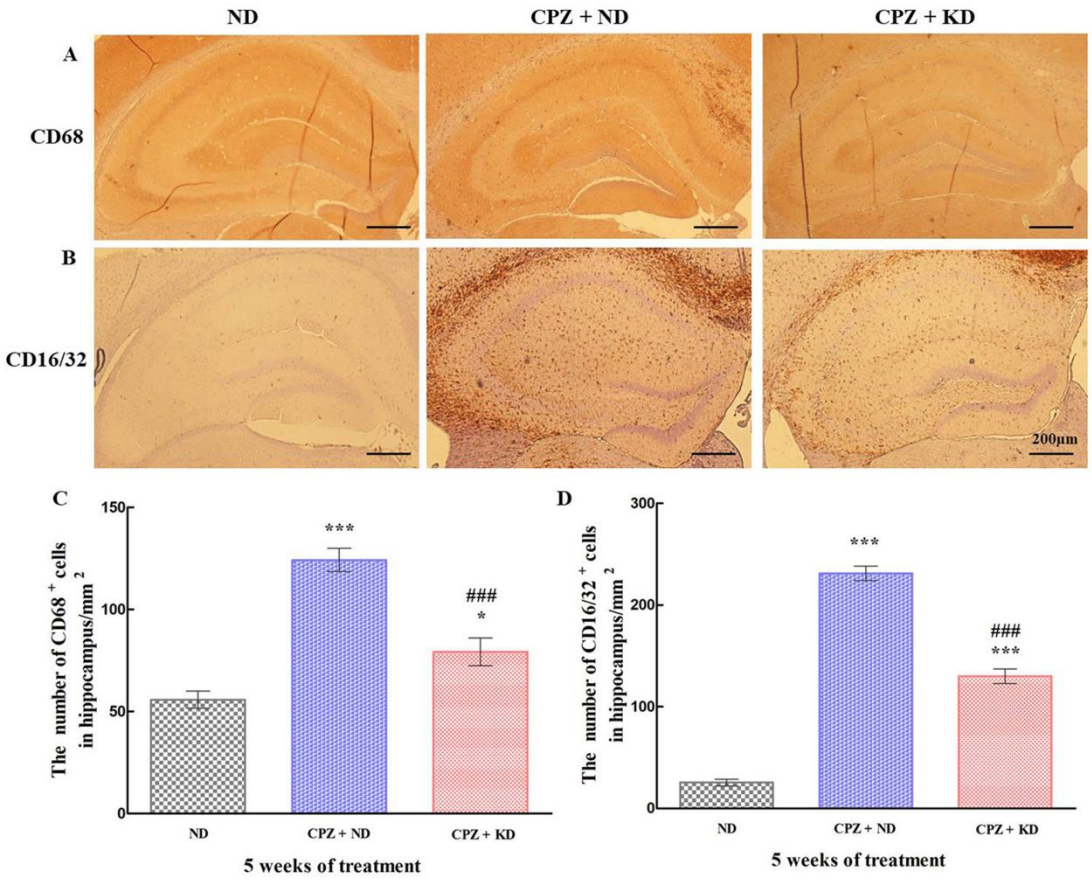
ND
CPZ + ND
CPZ + KD
A
CD68
B
CD16/32
200μm
C
The number of CD68+ cells in hippocampus/mm2
150
100
50
0
***
###
*
ND
CPZ + ND
CPZ + KD
5 weeks of treatment
D
The number of CD16/32+ cells in hippocampus/mm2
300
200
100
0
***
###
***
ND
CPZ + ND
CPZ + KD
5 weeks of treatment

Figure 6

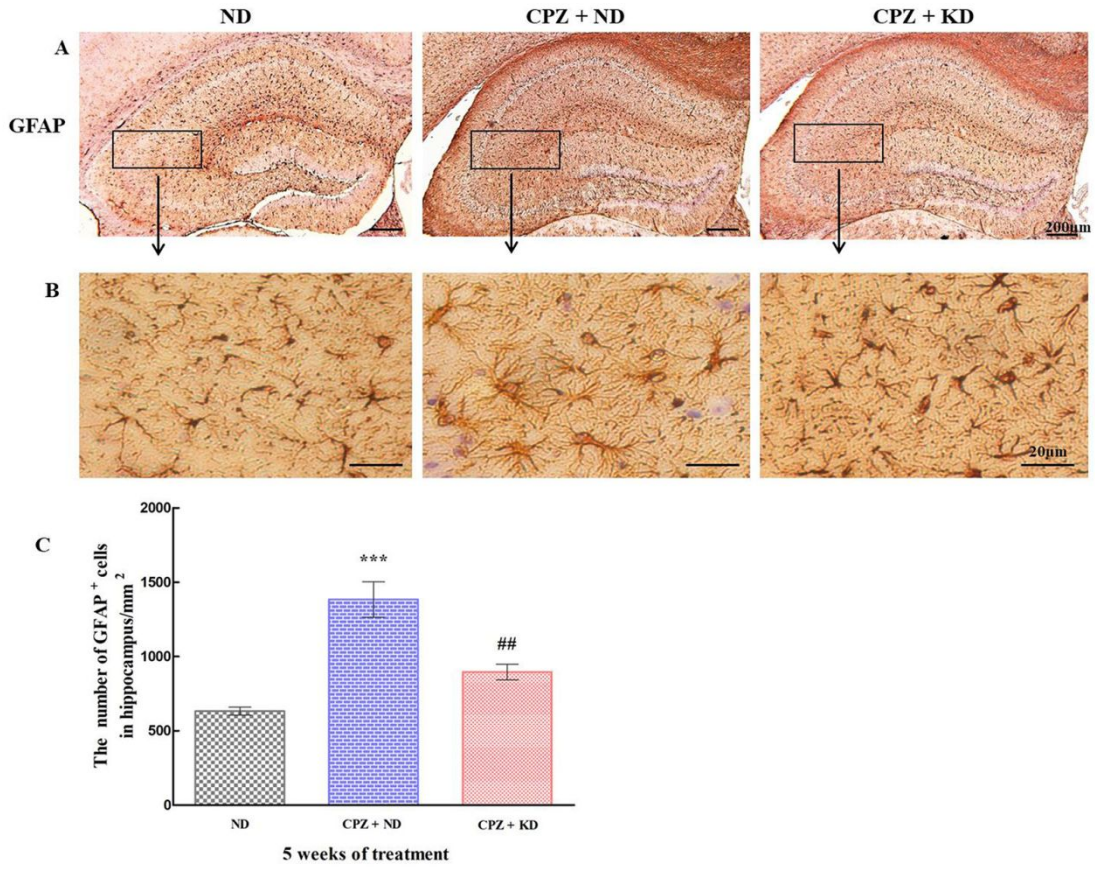
ND
CPZ + ND
CPZ + KD
A
GFAP
200μm
B
20μm
C
The number of GFAP+ cells in hippocampus/mm2
2000
1500
1000
500
0
***
##
ND
CPZ + ND
CPZ + KD
5 weeks of treatment

Figure 7

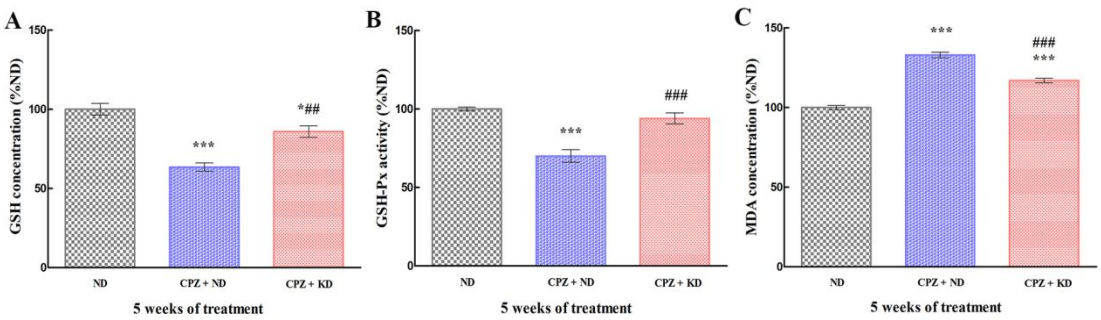
A
GSH concentration (%ND)
150
100
50
0
***
*##
ND
CPZ + ND
CPZ + KD
5 weeks of treatment
B
GSH-Px activity (%ND)
150
100
50
0
***
###
ND
CPZ + ND
CPZ + KD
5 weeks of treatment
C
MDA concentration (%ND)
150
100
50
0
***
###
***
ND
CPZ + ND
CPZ + KD
5 weeks of treatment

Figure 8

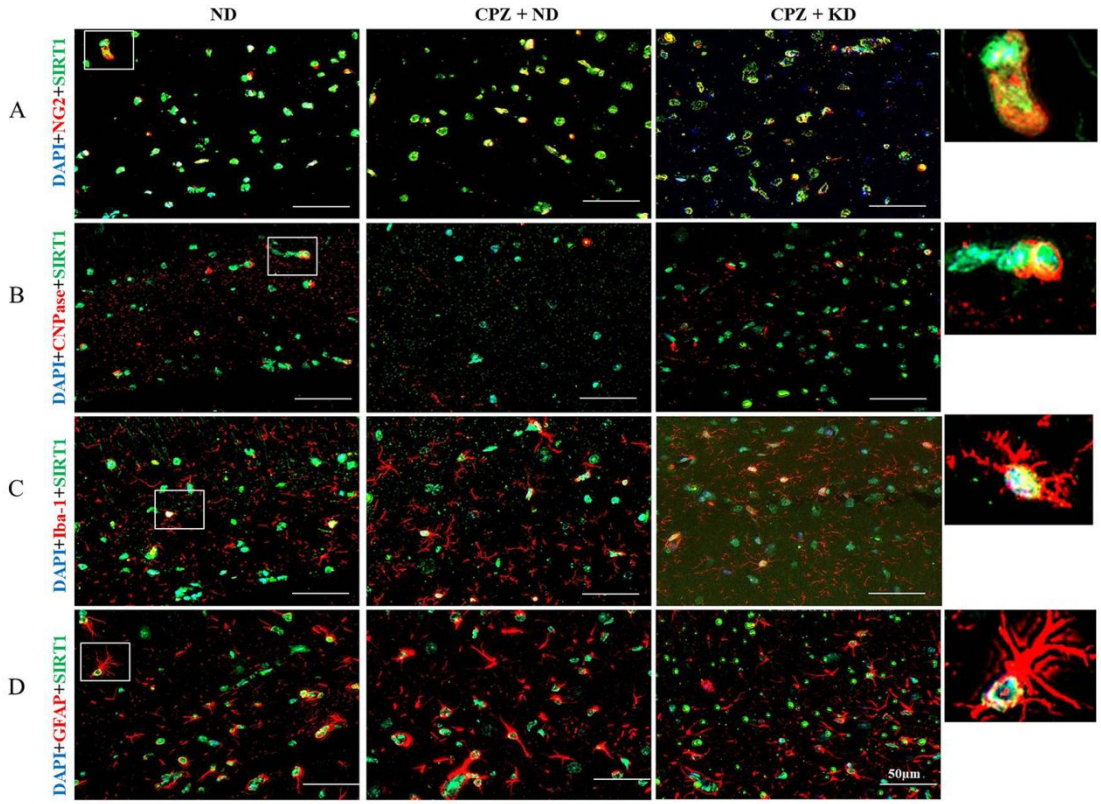
ND
CPZ + ND
CPZ + KD
A
DAPI+NG2+SIRT1
B
DAPI+CNPase+SIRT1
C
DAPI+Iba-1+SIRT1
D
DAPI+GFAP+SIRT1
50μm

Figure 9

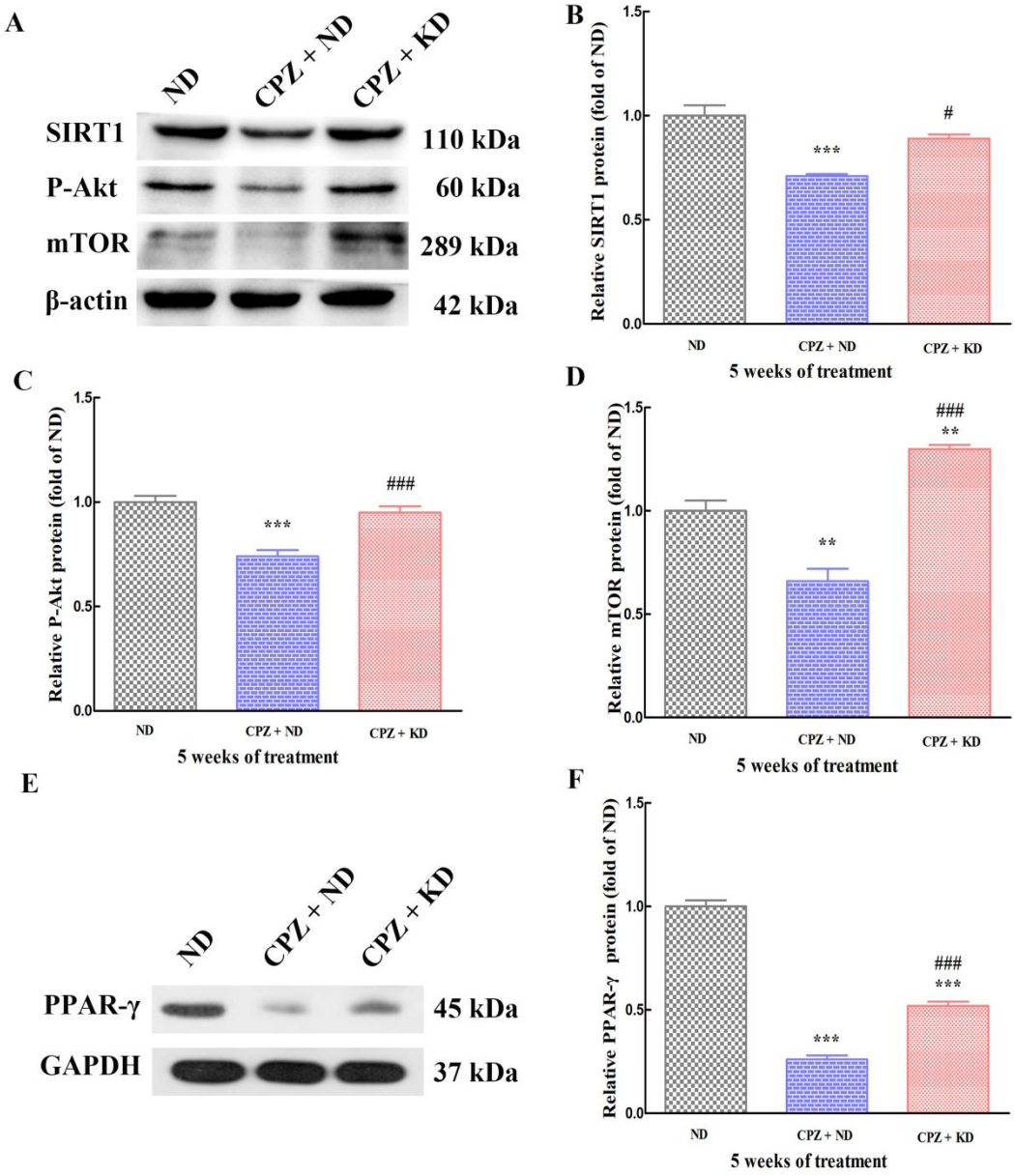
A
ND
CPZ + ND
CPZ + KD
SIRT1
110 kDa
P-Akt
60 kDa
mTOR
289 kDa
β-actin
42 kDa
B
Relative SIRT1 protein (fold of ND)
1.5
1.0
0.5
0.0
***
#
ND
CPZ + ND
CPZ + KD
5 weeks of treatment
C
Relative P-Akt protein (fold of ND)
1.5
1.0
0.5
0.0
***
###
ND
CPZ + ND
CPZ + KD
5 weeks of treatment
D
Relative mTOR protein (fold of ND)
1.5
1.0
0.5
0.0
**
###
**
ND
CPZ + ND
CPZ + KD
5 weeks of treatment
E
ND
CPZ + ND
CPZ + KD
PPAR-γ
45 kDa
GAPDH
37 kDa
F
Relative PPAR-γ protein (fold of ND)
1.5
1.0
0.5
0.0
***
###
***
ND
CPZ + ND
CPZ + KD
5 weeks of treatment

Figure 10

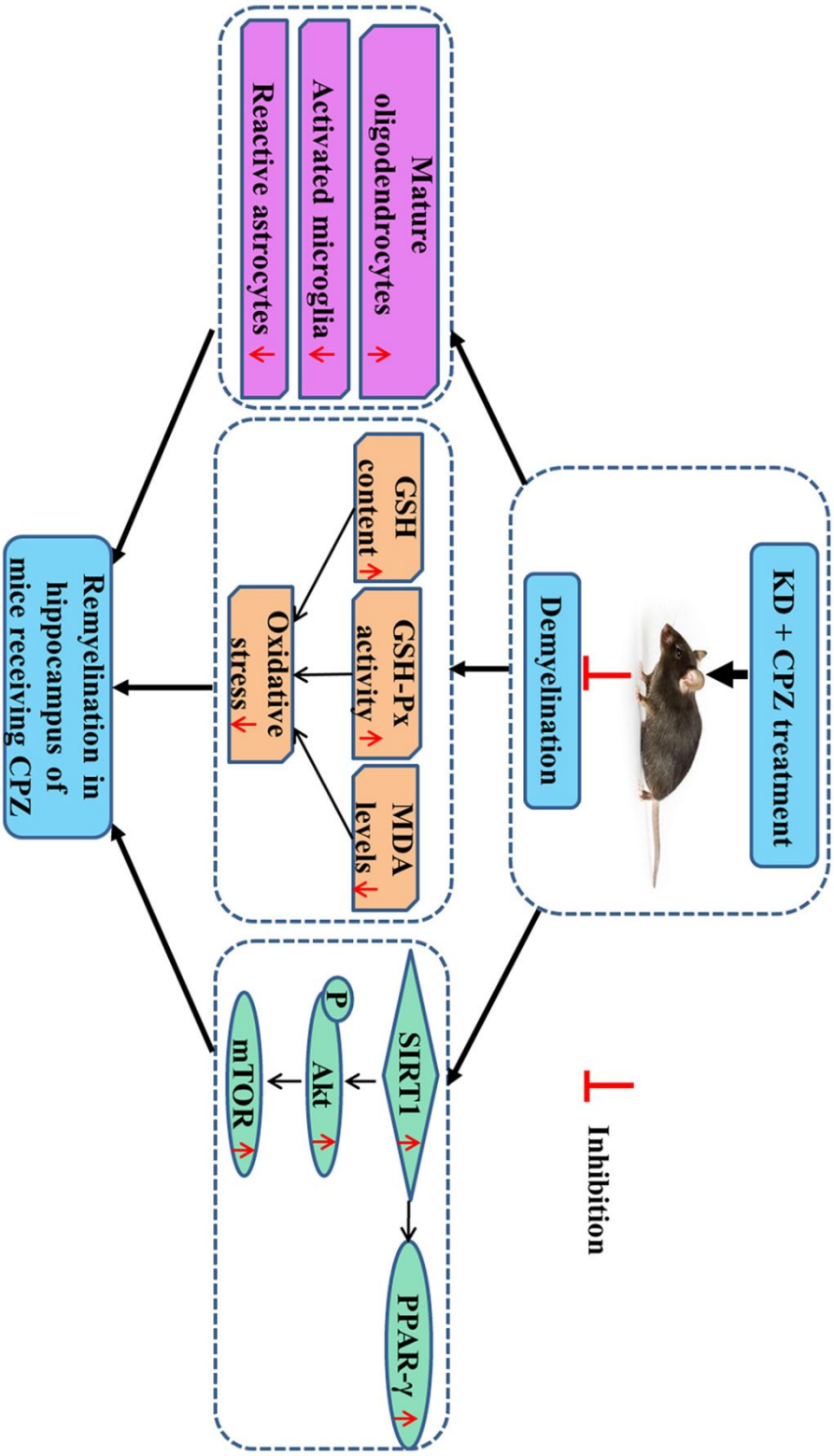

Graphical abstract